RHPN2 Drives Mesenchymal Transformation in Malignant Glioma by Triggering RhoA Activation

Carla Danussi[1,7], **Uri David Akavia**[2,3,7], **Francesco Niola**[1,#], **Andreja Jovic**[2], **Anna Lasorella**[1,4,5], **Dana Pe'er**[2,3,8,*], and **Antonio Iavarone**[1,5,6,8,*]

[1]Institute for Cancer Genetics, Columbia University Medical Center, New York, NY 10032, USA

[2]Department of Biological Sciences, Columbia University, New York, NY 10027, USA

[3]Center for Computational Biology and Bioinformatics, Columbia University Medical Center, New York, NY 10032, USA

[4]Department of Pediatrics, Columbia University Medical Center, New York, NY 10032, USA

[5]Department of Pathology, Columbia University Medical Center, New York, NY 10032, USA

[6]Department of Neurology, Columbia University Medical Center, New York, NY 10032, USA

Summary

Mesenchymal (MES) transformation is a hallmark of aggressive glioblastoma (GBM). Here we report the development of an unbiased method for computational integration of copy number variation, expression and mutation data from large datasets. Using this method we identified RHPN2 as a central genetic determinant of the MES phenotype of human GBM. Notably, amplification of the human RHPN2 gene on chromosome 19 correlates with a dramatic decrease in the survival of glioma patients. Ectopic expression of RHPN2 in neural stem cells and astrocytes triggered the expression of MES genes and promoted an invasive phenotype without impacting cell proliferation. Mechanistically, these effects were implemented through RHPN2-mediated activation of RhoA, a master regulator of cell migration and invasion. Our results define RHPN2 amplification as a central genetic determinant of a highly aggressive phenotype that directs the worst clinical outcomes in GBM patients.

Introduction

Glioblastoma multiforme (GBM) is the most common malignant brain tumor and is characterized by rapidly dividing cells, resistance to apoptosis, robust angiogenesis and extensive invasion. The tendency for local invasion leads to wide dissemination within the normal brain tissue surrounding the tumor, and to the formation of new malignant foci (1). As a consequence, complete tumor resection is almost impossible, leading to inevitable recurrence after surgery (2). Growing molecular evidence suggests that effective therapies

against GBM should target the deregulated signaling pathways that promote cell migration and invasion (3, 4), highlighting the need to identify specific genes driving these functional abnormalities.

Malignant transformation in glioma results from the accumulation of genetic aberrations, leading to complex and heterogeneous tumor phenotypes (5). Studies of genomic characterization, including copy number alterations, gene expression, mutations and methylation have all been used to identify molecular subclasses of malignant glioma that could inform clinical outcome and predict response to therapy (6–8). The reported classifications of GBM have invariably recognized a mesenchymal (MES) gene expression signature in patients with poor clinical prognosis (6–8). The MES signature includes genes related to the extracellular matrix (ECM), cell adhesion, migration, and tumor angiogenesis. A second signature, the Proneural signature, was identified in patients with a more favorable clinical outcome (9). The Proneural signature is characterized by genes associated with neurogenesis and is negatively correlated with the MES signature. Further studies of adult and pediatric GBM described the existence of a third signature, the Proliferative one, which is enriched for cell proliferation genes and their expression is also associated with a poor clinical outcome (6, 10, 11). However, the relationship between the Proliferative signature and the other two signatures is not entirely clear.

Multiple transcription factors have been implicated in controlling the MES signature. Gene expression network analysis identified the transcription factors *STAT3* and *C/EBP*β as two genetically normal genes that drive the MES signature in GBM (12). More recently, it has been shown that the transcriptional co-activator *TAZ* promotes MES transformation in malignant glioma (13). However, beside genetic alterations of NF1 that are associated with a small subgroup of MES GBM (7), the genetic drivers of the MES signature in malignant brain tumors remain largely unknown. Furthermore, whereas previous studies identified transcription factors triggering MES gene expression, genetic and/or epigenetic changes in key signaling pathway molecules driving the MES phenotype in GBM have not been identified.

Here, we report on the development of Multi-Reg, a new algorithm that integrates copy number aberrations, expression, and mutation data towards identifying driver genes, and describe its application to data of human GBM collected by TCGA. A key feature of Multi-Reg is that it associates each driver gene with the GBM subclass it induces. This approach identified Rhophilin 2 (*RHPN2*) as a novel driver gene of the MES signature. Experimental follow-up established that *RHPN2* promotes the MES transformation of neural stem cells and increases migration and invasion in different glial cell models. Importantly, *RHPN2* amplification and overexpression correlate with a dramatic decrease in the survival of glioma patients, supporting the involvement of this protein in the most aggressive features of malignant glioma.

Materials and Methods

Identification of Drivers

A detailed description of the computational algorithms used can be found in the Supplementary Methods section. The Multi-Reg algorithm was developed for this research, and the software is available at: http://www.c2b2.columbia.edu/danapeerlab/html/software.html.

Cell lines and cell culture conditions

SF188, SNB19 and 293T cell lines were grown in DMEM plus 10% FBS (Gibco/BRL). Primary human astrocytes (Lonza Inc.) were grown in Astrocyte Medium (SciencCell). Mouse NSCs (clone C17.2)(14) were cultured in DMEM plus 10% heat-inactivated FBS (Gibco/BRL), 5% horse serum (Gibco/BRL) and 1% l-glutamine (Gibco/BRL). Neuronal differentiation of mouse NSCs was induced by growing cells in DMEM supplemented with 0.5% horse serum.

Lentivirus infection

Lentiviral expression vectors pLOC *RHPN2* and pLOC VEC; and lentiviral vectors carrying *RHPN2* shRNAs were purchased from Thermo Scientific Open Biosystems. To generate lentiviral particles, each expression plasmid was co-transfected with pCMV-dR8.91 and pCMV-MD2.G vectors into human embryonic kidney 293T cells using Fugene 6 (Roche). Lentiviral infections were performed as previously described (15).

qRT–PCR and microarray analysis

RNA was prepared with RiboPure kit (Ambion), and used for first-strand cDNA synthesis using random primers and SuperScript II Reverse Transcriptase (Invitrogen). qRT–PCR was performed using Power SYBR Green PCR Master Mix (Applied Biosystems). Primers are listed in Supplementary Data, Table S1. qRT–PCR results were analysed by the C_T method (16) using 18S as a housekeeping gene.

RNA amplification for mouse array analysis was performed with Illumina TotalPrep RNA Amplification Kit (Ambion). One-and-a-half micrograms of amplified RNA was hybridized on Illumina Mouse ref8 v2 expression BeadChip according to the manufacturer's instructions. Hybridization data was obtained with an iScan BeadArray scanner (Illumina) and pre-processed by variance stabilization and robust spline normalization implemented in the lumi package under the R-system (17).

Immunofluorescence

Cells were grown on polylysine (Sigma) treated glass cover slips and fixed with PBS 4% PFA for 15 min. Then, they were permeabilized (with PBS, 1% BSA, 0.1% Triton X-100, and 2% FCS) for 5 min and saturated with the blocking buffer (PBS, 1% BSA, and 2% goat serum) for 30 min. The primary and the following secondary antibodies were incubated at room temperature for 1 h. These were: SMA (mouse monoclonal, Sigma), βIII-tubulin (mouse monoclonal, Promega), fibronectin and Paxillin (mouse monoclonal, BD Biosciences), phospho-Cofilin (rabbit monoclonal, Cell Signaling), goat anti-mouse and

anti-rabbit Cy3 conjugated (Life Technologies). Actin cytoskeleton was stained with Alexa-Fluor 568 Phalloidin (Life Technologies) and nuclei were visualized with DAPI (Invitrogen). Images were acquired with Nikon A1R MP confocal microscope. Quantification of the fibronectin intensity staining in mouse NSCs was performed using NIH Image J software (http://rsb.info.nih.gov/ij/).

Cell assays

Wound healing assay—Exponentially growing cells were seeded (1.5×10^5) in a 24-well plate to create a dense monolayer and then scratched with a 200 ml tip. Serum-free medium was added after washing in PBS, and wound closure was monitored by taking pictures over time for 24 h.

Invasion assay—2×10^4 cells were added to the upper compartment of a 24-well BioCoat Matrigel Invasion Chamber (BD Biosciences) in serum-free DMEM. After 24 h, invading cells were fixed, stained with crystal violet 0.1% and counted. In invasion inhibition assays RhoA inhibitor I (C3 exoenzyme; Cytoskeleton, Inc.) at a concentration of 1 µg/ml was used.

Proliferation assay—Cell proliferation was evaluated by 3-(4,5-dimethyl-2-thiazolyl)-2,5-diphenyl-2H-tetrazolium bromide (MTT) assay. 5,000 cells/well were seeded in 96-well plates. At the indicated times, MTT solution (Sigma) in complete medium (0.28-mg/ml final concentration) was added and incubated at 37°C for 4 h. The medium was discarded, and the formazan salts were dissolved in 4 mM HCl, 0.1% NP40 in isopropanol. The colorimetric substrate was measured and quantified at 560 nm in an enzyme-linked immunosorbent assay plate reader.

RhoA activity assay

Exponentially growing cells were serum starved for 24 h, detached with Accutase solution (Innovative Cell Technologies Inc.) and adhered to FN-coated dishes (10 µg/ml; Sigma) for 30 min. Then, cells were lysed and 300 µg of protein was tested in a rhotekin-RBD bead pulldown assay (Rho Activation Assay Biochem Kit, Cytoskeleton Inc.) for 1 h at 4°C. After thorough washes, the samples were boiled for 5 min in Laemmli buffer to detach active GTP-bound Rho and then loaded on 4–20% SDS-PAGE gels (Invitrogen) and immunoblotted using an anti-RhoA antibody.

Results

The Multi-Reg algorithm

An emerging trend in cancer treatment is drugs that target genes and signaling pathways that are only activated in specific cancer cells (18, 19). However, genomics has revealed incredible heterogeneity in cancer, which makes identification of specific genes contributing to cancer progression (driver genes) difficult. Targeting novel drivers is especially important in GBM, since the median survival with conventional therapy is 12–15 months (5).

A key challenge in identifying driver genes from DNA copy number is that amplification and deletions frequently involve large regions of DNA, each consisting of multiple genes. To pinpoint the driver genes within such genomic regions, we previously developed CONEXIC (20), a computational algorithm that integrates copy number and gene expression data, to identify driver genes and connect these to their expression signatures. A key limitation to our previous approach is that CONEXIC can only identify the one dominant driver for each expression signature. However, multiple drivers can contribute to the same effect, sometimes acting in parallel. For example, almost all GBM patients have activated Receptor Tyrosine Kinase signaling and disrupted *p53/RB* signaling, but each patient could have a different combination of deletions, amplifications and mutations in some of the many genes known to influence these signaling pathways (21).

We therefore developed Multi-Reg, based on a similar framework as CONEXIC, but seeking **multi**ple **reg**ulators for each phenotype. This improvement was achieved by a change in the main statistical model. While CONEXIC and other methods begin from gene expression signatures and attempt to find a driver for each one (22), Multi-Reg begins from candidate drivers and then finds a signature associated with each driver.

Multi-Reg begins from regions that are significantly altered in copy number, either amplified or deleted (Fig. 1A). It identifies all genes in each region as candidate driver genes (Fig. 1B). Then for each candidate driver it generates its gene expression signatures. i.e. the list of candidate target genes associated with this driver. Comparing the expression signatures between drivers from the same region allows us to focus on significant drivers (Fig. 1C). The final step of the analysis involves assigning the expression signature of each predicted driver to a distinct subtype of GBM (MES, Proliferative, Proneural). This leads to the testable hypothesis that some genes altered in copy number are drivers of distinct biological functions and the same region may contain multiple drivers that effect distinct GBM subtypes (Fig. 1D). More details on the algorithm can be found in the Supplementary Methods.

Identifying drivers in glioblastoma

We analyzed gene expression and copy number measurements from 136 samples (corrected for batch effects) of primary GBM from the TCGA cohort (21), see Supplementary Methods for details. We identified 238 regions that are recurrently altered in copy number using a modified version of GISTIC called JISTIC (23) and generated a list of 747 candidate drivers contained within these regions. Next, we applied Multi-Reg to integrate copy number with gene expression and mutation data to pinpoint the top ranking candidate drivers and their targets. Applying Multi-Reg resulted in the identification of 83 high-scoring drivers, which associate with a total of 12125 targets.

Multi-Reg identified many of the well-known oncogenes and tumor suppressors in GBM, including *EGFR, NF1, CKDN2B, p53, PIK3CA, RB1, PTEN* (21), and more (see Table S2 for complete list). The successful identification of known key brain tumor drivers increases our confidence in the novel predictions discussed below. To determine the functional properties of the identified drivers, we compared the gene expression signatures previously associated with MES, Proneural and Proliferative GBM subtypes (12) with the gene

modules associated with each driver identified by Multi-Reg, using hypergeometric enrichment.

In addition to well-known drivers of GBM, we identified new drivers that regulate the GBM signatures. Overall, out of the 83 drivers we identified, 23 drivers were associated with the MES, 14 with the Proliferative and 11 with the Proneural signature (Table S2 for all drivers and see Fig. 2A and B for a schematic representation of these 48 drivers and the chromosomal location of the drivers associated with the MES signature). Thus our algorithm is able to identify drivers for each of the three crucial GBM subtypes.

Multi-Reg identifies *RHPN2* as an amplified driver of the MES subclass

We focused on the genes implicated in the Mesenchymal subtype, since this subtype has the worst clinical prognosis. We sorted the 23 genes associated with the MES signature according to q-value. The top three genes, *ERBB2*, *COL1A1* and *ITGB3,* were mutated, but they did not harbor copy number changes. The next two top genes, *C5orf32* and *RHPN2,* were both amplified and overexpressed. The *RHPN2* gene is located on Chr19q12-q13 and, according to data from TCGA and Rembrandt databases, it is amplified and overexpressed in >30% of gliomas (Fig. S2). This gene codes for a RhoA-binding protein, called Rhophilin 2, which is not well characterized. We focused further experiments on *RHPN2*, given its potential biological function as regulator of Rho GTPases (24), which are key factors for cell migration and invasion, two hallmarks of the MES phenotype.

To further investigate the genes associated with this driver, we used Gene Ontology enrichment to analyze the function of predicted up- or down-regulated target genes identified by Multi-Reg for *RHPN2* (Fig. 3). We found that *RHPN2* up-regulated genes were significantly enriched for plasma membrane, extracellular region, transmembrane transporter activity, regulation of protein kinase cascade and cell adhesion (Fig. 3A and B), indicating that *RHPN2* regulates the expression of genes involved in cell-ECM interactions, which is consistent with the induction of a MES phenotype. Genes down-regulated by *RHPN2* were significantly enriched for the Gene Ontology terms such as development, neuron projection morphogenesis, regulation of gene expression and glial cell differentiation (Fig. 3C and D) and for the Proneural signature (q-value = 5.33×10^{-13}). Thus, the Gene Ontology results match the predictions based on GBM signatures, *RHPN2* induces a MES phenotype while repressing neuronal and glial cell differentiation.

A survival study performed in the Rembrandt database supported the importance of RHPN2 in GBM and encouraged us to investigate the role of this protein. According to this analysis, RHPN2 amplification and overexpression predicts a markedly poor clinical outcome of glioma patients (Fig. 3E). Among the top ranked drivers selected by Multi-Reg and associated with the MES genes, RHPN2 displayed the strongest statistical association with patient survival (data not shown).

To experimentally validate the new driver for GBM aggressiveness inferred by the Multi-Reg algorithm, we performed biological assays, overexpressing and/or silencing *RHPN2* in different cell models. We started by testing the expression of specific genes and proteins that

are representative of GBM phenotypes, performed functional assays and finally explored in detail the mechanism of action of *RHPN2*.

RHPN2 triggers mesenchymal transformation of Neural Stem Cells

We used recombinant lentiviruses to express *RHPN2* in C17.2 (Fig. S3A), a mouse immortalized neural stem cell (NSC) line previously used to investigate MES transformation of high-grade glioma (12). Consistent with the computational predictions, microarray gene expression analyzed by GSEA showed that expression of *RHPN2* in C17.2 led to significant enrichment of MES genes (Fig. 4A; p-value = 0.0003). This result was validated by quantitative-RT-PCR of a representative panel of MES genes. *Acta1, Acta2, Ctgf, Tnc, SerpinE1, Itga7, Osmr and C1rl* were up-regulated after ectopic expression of *RHPN2* (Fig. 4B). In addition, *RHPN2* triggered the expression of MES proteins as shown by immunostaining for the MES markers fibronectin (FN) and smooth muscle alpha actin (SMA, encoded by the *Acta2* gene; Fig. 4C–F; p-value $< 1 \times 10^{-4}$).

Next, we asked whether *RHPN2* altered the default neuronal differentiation pathway of NSCs. Normally, C17.2 NSCs undergo neuronal differentiation upon mitogen removal (14). However, ectopic expression of *RHPN2* conferred a fibroblast-like morphology (Fig. 4G) and inhibited neuronal differentiation, as evidenced by a decrease in βIII-tubulin immunostaining (Fig. 4H–I, p-value $< 1 \times 10^{-4}$). These findings suggest that *RHPN2* blocks neuronal differentiation by reprogramming NSCs towards an aberrant MES lineage.

RHPN2 increases invasion in Neural Stem Cells and glioma cell lines

To elucidate the full scope of the biological phenotypes triggered by *RHPN2*, we used both gain and loss of function experiments. Based on the Multi-Reg predictions about the MES phenotype, we focused on invasion and migration assays. In addition to mouse NSCs we used primary Human Astrocytes (HA), candidate cells-of-origin for GBM, and two human glioma cell lines, SF188 and SNB19, which display the lowest and highest *RHPN2* expression levels among several glioma cell lines respectively (Fig. S3B). One of the most distinguishing features of MES transformation is increased invasiveness (12). Indeed, expression of *RHPN2* in C17.2 cells promoted invasion through the extracellular matrix in a Matrigel invasion assay (Fig. 5A) and enhanced cell migration in a wound assay (Fig. 5B). Interestingly, ectopic expression of *RHPN2* (Fig. S3C) resulted in dramatic changes of the morphology of HA. Compared to control vector infected cells, HA expressing *RHPN2* acquired an elongated and spindle-shaped morphology (Fig. S3D). Notably, these changes were associated with increased ability to invade through Matrigel (Fig. 5C; p-value < 0.001). A significant gain of invasion was observed also when *RHPN2* was introduced in SF188 cells (Fig. S3E and 5D, p-value $< 1 \times 10^{-5}$). Conversely, silencing of *RHPN2* in the human glioma cell line SNB19 by 4 different shRNA sequences (Fig. S3F) significantly decreased the invasive capacity through Matrigel (Fig. 5E; p-value < 0.005). Neither the ectopic expression of *RHPN2* in HA and SF188 or its silencing in SNB19 affected cell proliferation (Fig. 5F–H).

Altogether these data indicate that RHPN2 overexpression is sufficient and necessary to drive transformation of glioma cells along the MES lineage.

RHPN2 promotes invasion by activation of RhoA

We sought to identify the molecular mechanisms by which *RHPN2* amplification/ overexpression generates MES transformation of glial cells. To address this question, we first asked whether *RHPN2* affects RhoA activity in primary human astrocytes (HA). We selected astrocytes as appropriate cellular models for the next series of experiments, since they are candidate cells-of-origin for GBM and display low rates of invasion. Ectopic expression of *RHPN2* (Fig. S3C) resulted in more than 4-fold increase of RhoA activity (measured as RhoA-GTP), when compared with control cells (Fig. 6A).

Next, we asked whether the increase in RhoA activity by *RHPN2* affected organization of the actin cytoskeleton, a key determinant of cell migration and invasion. After 30 min of adhesion on fibronectin, vector-transduced HA displayed a well-organized network of actin stress fibers that were distributed in the whole cell body (Fig. 6B, upper panel). *RHPN2*-expressing cells manifested a profound reorganization of the actin cytoskeleton, characterized by lack of stress fibers and accumulation of actin at the cell border in a ring-shaped manner, resembling a non-polarized lamellipodium (Fig. 6B, lower panel). Immunostaining for Paxillin, a protein implicated in cell migration (25), showed the expected localization of this protein at the focal contacts in control cells (Fig. 6B, upper panel). However, in HA transduced with the *RHPN2*-expressing lentivirus Paxillin formed concentric circles at the cell edge, co-localizing with actin (Fig. 6B, lower panel). Moreover, the aberrant activation of the RhoA pathway by *RHPN2* resulted in the accumulation of membrane speckles of phospho-Cofilin (pCofilin; Fig. 6B), a downstream effector of RhoA (26).

Finally, we asked whether the increased RhoA activity induced by *RHPN2* was responsible for the enhanced cell invasion. Treatment of vector and *RHPN2*-expressing cells with a specific RhoA inhibitor (named RhoA inhibitor I or C3 exoenzyme) completely abrogated RhoA activity after 6 hours (Fig. 6C). An invasion assay revealed that inhibition of RhoA did not affect the basal invasion capacity of HA transduced with the control lentivirus, but it completely reversed the *RHPN2*-induced invasion (Fig. 6D; p-value $< 3 \times 10^{-5}$). Together, these results indicate that activation of RhoA is specifically recruited to enhance invasion of HA following ectopic expression of *RHPN2*.

Discussion

Malignant transformation in gliomas results from the accumulation of genetic aberrations and the deregulation of several key signaling pathways (5). The advent of genome-wide profiling studies of one data type at a time led to the identification of certain driver genes involved in glioma malignancy, but additional important insights can be gained by integrating multiple data. Existing methods for integration have generally found one regulator for a given gene expression signature (20, 22). Recent studies have shown success in identifying drivers based on copy number and expression, but only resulted in a limited number of targets (approximately 500 targets in total)(27).

Here, we presented a new algorithm called Multi-Reg, which improves on these existing methods, finds **multi**ple **reg**ulators for genes identified as targets, and associates each driver

gene with a relevant phenotype. Finding multiple regulators for each phenotype is a more accurate reflection of the biology of cancer, where many amplifications, deletions and mutations can influence the same signaling pathway (21).

We applied the Multi-Reg algorithm to a GBM dataset, and related our results to known subtypes of glioma. In addition to novel drivers, we correctly identified previously known drivers, thus increasing our confidence in our results. The novel drivers we identified were involved in all three glioma subtypes, including Proliferative, Proneural and MES.

Among all the genes selected by Multi-Reg, we focus on those that induce the MES phenotype, since they should correlate with a bad prognosis and could represent ideal potential therapeutic targets. In particular, we decided to deeply investigate *RHPN2*, a gene located on chromosome 19q12–13, which has been described as RhoA binding protein, but its biological function remained obscure (24, 28, 29). Importantly, Multi-Reg identified *RHPN2*, correctly predicted its resulting phenotype as a MES subclass inducer and let us shed light on its novel functional role as regulator of invasion in glioma. In accordance with the computational prediction, *RHPN2* ectopic expression in mouse NSCs induced the expression of MES genes, prevented neuronal differentiation and promoted invasion and migration, thus operating as a bona-fide master regulator of MES transformation. Notably, *RHPN2* expression was not sufficient for neoplastic transformation and did not affect other cell functions, such as proliferation. Altogether, these results indicate that RHPN2 amplification and overexpression are not implicated in glioma tumorigenesis, but most likely they represent a late event in glioma progression and significantly contribute to worse prognosis of the patients harboring this genetic aberration, as confirmed by a survival analysis (Fig. 3E).

It is important to note that pooled RNAi screens (30), a popular genome-wide technique that is focused on growth and proliferation, would not detect *RHPN2* as a driver, since *RHPN2* does not effect proliferation. Multi-Reg's ability to connect drivers with their phenotypes was a crucial feature in identifying the correct follow-up experiments and importantly it unveiled a new biological function of *RHPN2*.

We investigated in depth the mechanism of action of *RHPN2* and demonstrated that this protein promotes MES transformation by activating RhoA. Increased levels of RhoA-GTP and pCofilin, a downstream effector of RhoA, were detected in *RHPN2*-expressing cells. Notably, the invasive phenotype was reversed upon treatment with a specific RhoA inhibitor, indicating that the *RHPN2*-induced MES transformation resulted from aberrant RhoA activation.

RhoA is a member of the Rho GTPases, a family of proteins that play essential roles in multiple biological processes. In particular, their ability to regulate cytoskeletal dynamics, cell adhesion and cell migration points to a central role in cancer cell invasion and metastasis (31). The involvement of Rho family GTPases in glioma malignancy and invasion has been previously described, but the specific role of RhoA has remained controversial (reviewed by Khalil and El-Sibai (32)). Goldberg and Kloog (3) showed that glioma cell migration was blocked following treatment with a Ras inhibitor, and that this

effect was associated with decreased Rac-1 and increased RhoA activity. In contrast, Manning and colleagues (33) reported that blocking RhoA signaling could inhibit lysophosphatidic acid-induced migration in glioma cells. Our findings showed that RhoA activation is necessary for *RHPN2* induced glioma invasion, matching more closely the role of RhoA described in other cancer models (34) and highlighting RhoA as a potential therapeutic target of GBM. Our study also underlines the critical need to enhance the efforts to produce specific RhoA inhibitors for therapeutic applications, especially for tumors that lack effective therapies, such as GBM.

In conclusion, by developing a new integrated analysis and applying it to GBM, we identified a very frequent genetic aberration in this cancer that drives a gain in malignancy through the activation of a key regulator for the MES phenotype. Notably, this is the first report describing a MES driver that does not belong to the Transcription Factor category and unveiling the related molecular pathway. By disclosing the role of RhoA in MES transformation and glioma invasiveness, our work sets the stage for new therapeutic tools in mesenchymal GBM.

Supplementary Material

Refer to Web version on PubMed Central for supplementary material.

Acknowledgements

References

1. Schonsteiner SS, Bommer M, Haenle MM, Klaus B, Scheuerle A, Schmid M, et al. Rare phenomenon: liver metastases from glioblastoma multiforme. J Clin Oncol. 2011; 29:e668–e671. [PubMed: 21670450]

2. Giese A, Bjerkvig R, Berens ME, Westphal M. Cost of migration: invasion of malignant gliomas and implications for treatment. J Clin Oncol. 2003; 21:1624–1636. [PubMed: 12697889]

3. Goldberg L, Kloog Y. A Ras inhibitor tilts the balance between Rac and Rho and blocks phosphatidylinositol 3-kinase-dependent glioblastoma cell migration. Cancer Res. 2006; 66:11709–11717. [PubMed: 17178866]

4. Feng H, Hu B, Liu KW, Li Y, Lu X, Cheng T, et al. Activation of Rac1 by Src-dependent phosphorylation of Dock180(Y1811) mediates PDGFRalpha-stimulated glioma tumorigenesis in mice and humans. J Clin Invest. 2011; 121:4670–4684. [PubMed: 22080864]

5. Wen PY, Kesari S. Malignant Gliomas in Adults. New England Journal of Medicine. 2008; 359:492–507. [PubMed: 18669428]

6. Phillips HS, Kharbanda S, Chen R, Forrest WF, Soriano RH, Wu TD, et al. Molecular subclasses of high-grade glioma predict prognosis, delineate a pattern of disease progression, and resemble stages in neurogenesis. Cancer Cell. 2006; 9:157–173. [PubMed: 16530701]

7. Verhaak RGW, Hoadley KA, Purdom E, Wang V, Qi Y, Wilkerson MD, et al. Integrated Genomic Analysis Identifies Clinically Relevant Subtypes of Glioblastoma Characterized by Abnormalities in PDGFRA, IDH1, EGFR, and NF1. Cancer Cell. 2010; 17:98–110. [PubMed: 20129251]

8. Sturm D, Witt H, Hovestadt V, Khuong-Quang D-A, Jones DTW, Konermann C, et al. Hotspot Mutations in H3F3A and IDH1 Define Distinct Epigenetic and Biological Subgroups of Glioblastoma. Cancer Cell. 2012; 22:425–437. [PubMed: 23079654]

9. Huse JT, Phillips HS, Brennan CW. Molecular subclassification of diffuse gliomas: seeing order in the chaos. Glia. 2011; 59:1190–1199. [PubMed: 21446051]

10. Freije WA, Castro-Vargas FE, Fang Z, Horvath S, Cloughesy T, Liau LM, et al. Gene expression profiling of gliomas strongly predicts survival. Cancer Res. 2004; 64:6503–6510. [PubMed: 15374961]

11. Paugh BS, Qu C, Jones C, Liu Z, Adamowicz-Brice M, Zhang J, et al. Integrated Molecular Genetic Profiling of Pediatric High-Grade Gliomas Reveals Key Differences With the Adult Disease. Journal of Clinical Oncology. 2010; 28:3061–3068. [PubMed: 20479398]

12. Carro MS, Lim WK, Alvarez MJ, Bollo RJ, Zhao X, Snyder EY, et al. The transcriptional network for mesenchymal transformation of brain tumours. Nature. 2010; 463:318–325. [PubMed: 20032975]

13. Bhat KP, Salazar KL, Balasubramaniyan V, Wani K, Heathcock L, Hollingsworth F, et al. The transcriptional coactivator TAZ regulates mesenchymal differentiation in malignant glioma. Genes Dev. 2011; 25:2594–2609. [PubMed: 22190458]

14. Parker MA, Anderson JK, Corliss DA, Abraria VE, Sidman RL, Park KI, et al. Expression profile of an operationally-defined neural stem cell clone. Exp Neurol. 2005; 194:320–332. [PubMed: 15992799]

15. Zhao X, Heng JI, Guardavaccaro D, Jiang R, Pagano M, Guillemot F, et al. The HECT-domain ubiquitin ligase Huwe1 controls neural differentiation and proliferation by destabilizing the N-Myc oncoprotein. Nat Cell Biol. 2008; 10:643–653. [PubMed: 18488021]

16. Livak KJ, Schmittgen TD. Analysis of relative gene expression data using real-time quantitative PCR and the 2(-Delta Delta C(T)) Method. Methods. 2001; 25:402–408. [PubMed: 11846609]

17. Du P, Kibbe WA, Lin SM. lumi: a pipeline for processing Illumina microarray. Bioinformatics. 2008; 24:1547–1548. [PubMed: 18467348]

18. Burris HA 3rd, Rugo HS, Vukelja SJ, Vogel CL, Borson RA, Limentani S, et al. Phase II study of the antibody drug conjugate trastuzumab-DM1 for the treatment of human epidermal growth factor receptor 2 (HER2)-positive breast cancer after prior HER2-directed therapy. J Clin Oncol. 2011; 29:398–405. [PubMed: 21172893]

19. Flaherty KT, Puzanov I, Kim KB, Ribas A, McArthur GA, Sosman JA, et al. Inhibition of mutated, activated BRAF in metastatic melanoma. N Engl J Med. 2010; 363:809–819. [PubMed: 20818844]

20. Akavia UD, Litvin O, Kim J, Sanchez-Garcia F, Kotliar D, Causton HC, et al. An Integrated Approach to Uncover Drivers of Cancer. Cell. 2010; 143:1005–1017. [PubMed: 21129771]

21. Cancer Genome Atlas Research Network. Comprehensive genomic characterization defines human glioblastoma genes and core pathways. Nature. 2008; 455:1061–1068. [PubMed: 18772890]

22. Adler AS, Lin M, Horlings H, Nuyten DS, van de Vijver MJ, Chang HY. Genetic regulators of large-scale transcriptional signatures in cancer. Nat Genet. 2006; 38:421–430. [PubMed: 16518402]

23. Sanchez-Garcia F, Akavia UD, Mozes E, Pe'er D. JISTIC: Identification of Significant Targets in Cancer. BMC Bioinformatics. 2010; 11:189. [PubMed: 20398270]

24. Peck JW, Oberst M, Bouker KB, Bowden E, Burbelo PD. The RhoA-binding protein, rhophilin-2, regulates actin cytoskeleton organization. J Biol Chem. 2002; 277:43924–46932. [PubMed: 12221077]

25. Schaller MD. Paxillin: a focal adhesion-associated adaptor protein. Oncogene. 2001; 20:6459–6472. [PubMed: 11607845]

26. Toshima J, Toshima JY, Amano T, Yang N, Narumiya S, Mizuno K. Cofilin phosphorylation by protein kinase testicular protein kinase 1 and its role in integrin-mediated actin reorganization and focal adhesion formation. Mol Biol Cell. 2001; 12:1131–1145. [PubMed: 11294912]

27. Jornsten R, Abenius T, Kling T, Schmidt L, Johansson E, Nordling TE, et al. Network modeling of the transcriptional effects of copy number aberrations in glioblastoma. Mol Syst Biol. 2011; 7:486. [PubMed: 21525872]

28. Chen Y, Sheng R, Kallberg M, Silkov A, Tun MP, Bhardwaj N, et al. Genome-wide functional annotation of dual-specificity protein- and lipid-binding modules that regulate protein interactions. Mol Cell. 2012; 46:226–237. [PubMed: 22445486]

29. Steuve S, Devosse T, Lauwers E, Vanderwinden JM, Andre B, Courtoy PJ, et al. Rhophilin-2 is targeted to late-endosomal structures of the vesicular machinery in the presence of activated RhoB. Exp Cell Res. 2006; 312:3981–3989. [PubMed: 17054945]

30. Zender L, Xue W, Zuber J, Semighini CP, Krasnitz A, Ma B, et al. An Oncogenomics-Based In Vivo RNAi Screen Identifies Tumor Suppressors in Liver Cancer. Cell. 2008; 135:852–864. [PubMed: 19012953]

31. Vega FM, Ridley AJ. Rho GTPases in cancer cell biology. FEBS Lett. 2008; 582:2093–2101. [PubMed: 18460342]

32. Khalil BD, El-Sibai M. Rho GTPases in primary brain tumor malignancy and invasion. J Neurooncol. 2012; 108:333–339. [PubMed: 22528793]

33. Manning TJ Jr, Parker JC, Sontheimer H. Role of lysophosphatidic acid and rho in glioma cell motility. Cell Motil Cytoskeleton. 2000; 45:185–199. [PubMed: 10706774]

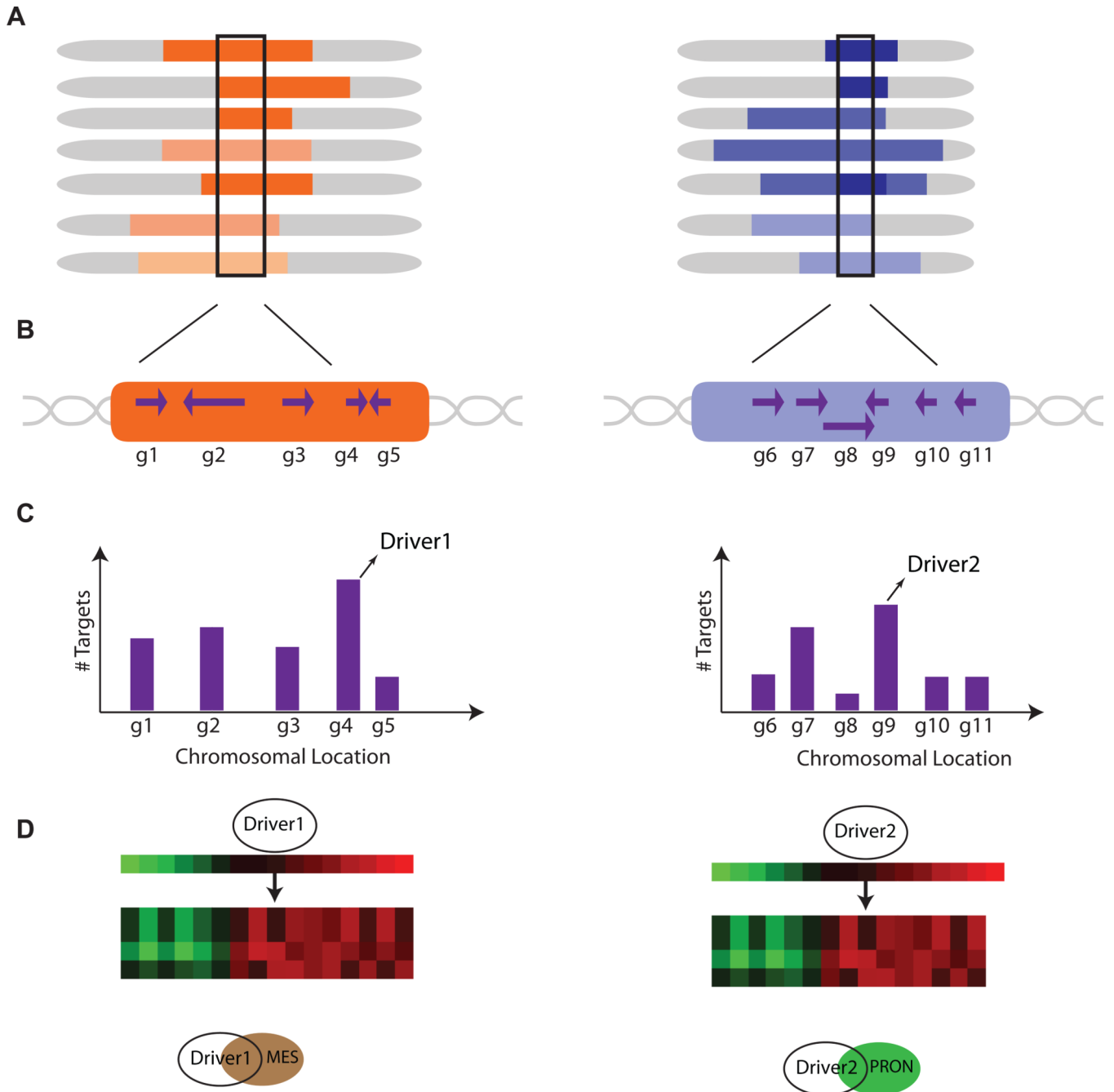34. Sahai E, Marshall CJ. RHO-GTPases and cancer. Nat Rev Cancer. 2002; 2:133–142. [PubMed: 12635176]

Figure 1. Principles of the algorithm Multi-Reg

(A) Copy Number allows us to identify specific amplified (in orange) or deleted (in blue) chromosomal regions.
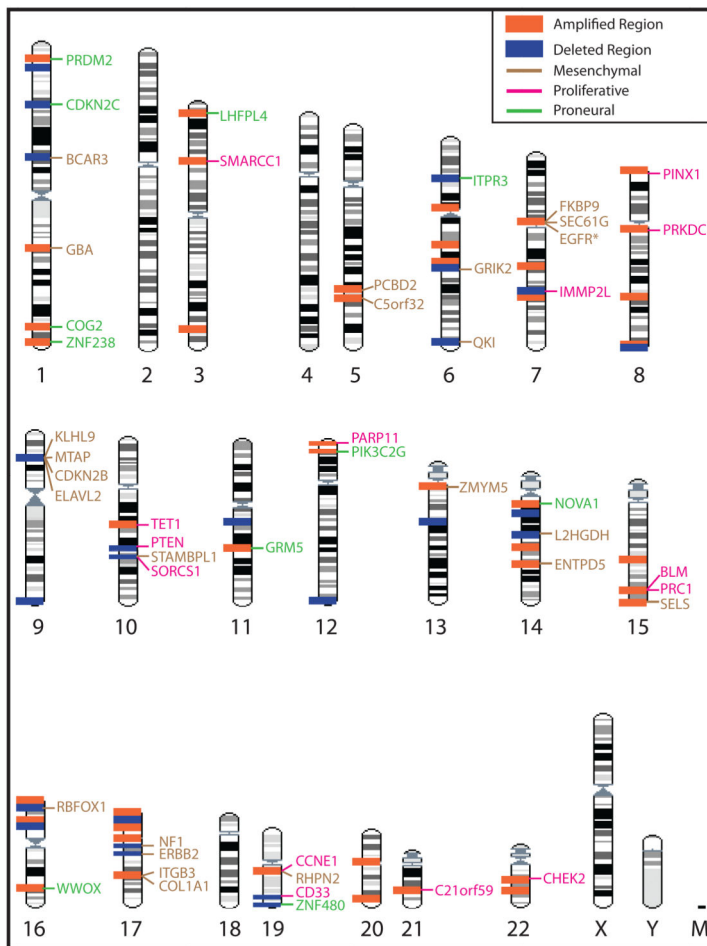
(B) Each chromosomal region includes multiple genes (genes are identified as g1..g5 for the amplified region and g6..g10 for the deleted region).

(C) Combining expression allows us to focus on fewer drivers in each region. We can measure the effect each gene has on expression (see Supplementary Materials for more details), and identify candidate drivers. The purple bars represent the number of targets

identified. Genes in the region with more than a minimum of targets are identified as the candidate driver for that region (arrows).

(D) The overlap between the targets of each driver with known GBM signatures allows us to identify the function of the driver. If most of the targets of a driver overlap with the mesenchymal signature (MES; left), we will assume the driver contributes to the mesenchymal phenotype. Similarly, if the targets of the driver overlap with the Proneural signature (PRON; right), we will assume it contributes to the proneural phenotype.

Figure 2. Multi-Reg identifies multiple regions and genes

(A) Graphical representation of chromosomes with amplified and deleted regions (orange and blue, respectively). Genes identified as candidate drivers are noted and colored according to their signature, Mesenchymal (brown), Proneural (green) and Proliferative (pink).

(B) List of driver genes identified by MultiReg and significantly associated with a GBM signature class, sorted by class and q-value. In the table chromosomal location, gene symbol, GBM signature and q-value are reported. * EGFR represses proneural with the q-value listed.
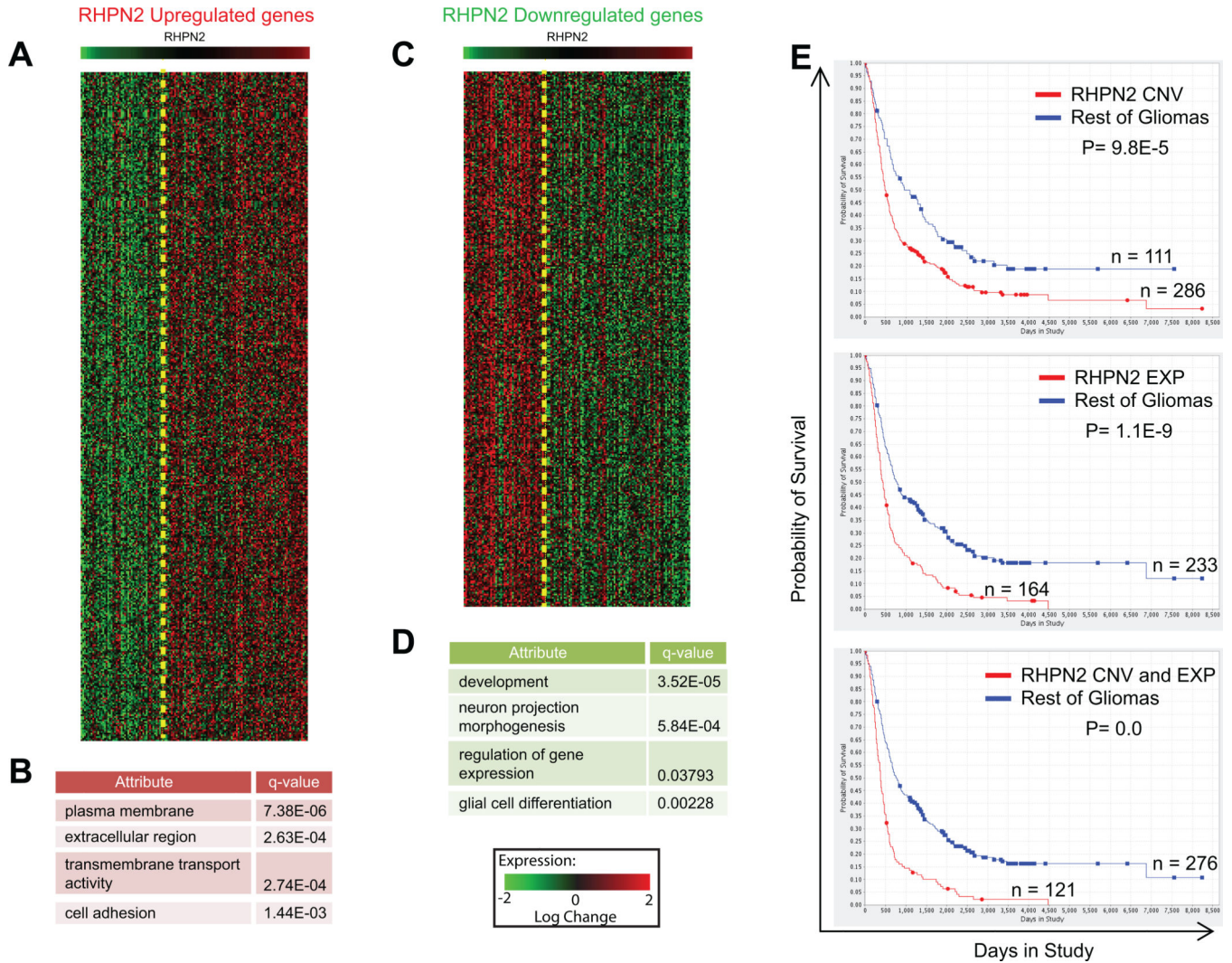
RHPN2 Upregulated genes

A

RHPN2 Downregulated genes

C

E

Attribute	q-value
plasma membrane	7.38E-06
extracellular region	2.63E-04
transmembrane transport activity	2.74E-04
cell adhesion	1.44E-03

B

D

Attribute	q-value
development	3.52E-05
neuron projection morphogenesis	5.84E-04
regulation of gene expression	0.03793
glial cell differentiation	0.00228

Expression:
-2   0   2
Log Change

Days in Study

Figure 3. *RHPN2* **module analysis**

(A) Module of *RHPN2* up-regulated genes generated by Multi-Reg.

(B) Gene Ontology (GO) enrichment for *RHPN2* up-regulated genes. *RHPN2* up-regulated genes are related to cell-ECM interactions.

(C) Module of *RHPN2* down-regulated genes generated by Multi-Reg

(D) GO enrichment for *RHPN2* down-regulated genes. *RHN2* down-regulated genes are related to glial cell differentiation.

(E) Survival analysis of glioma patients from Rembrandt database. Each plot represents the probability of survival of glioma patients in correlation with CNV (copy number variation 2), EXP (gene expression 2) and the combination of both.
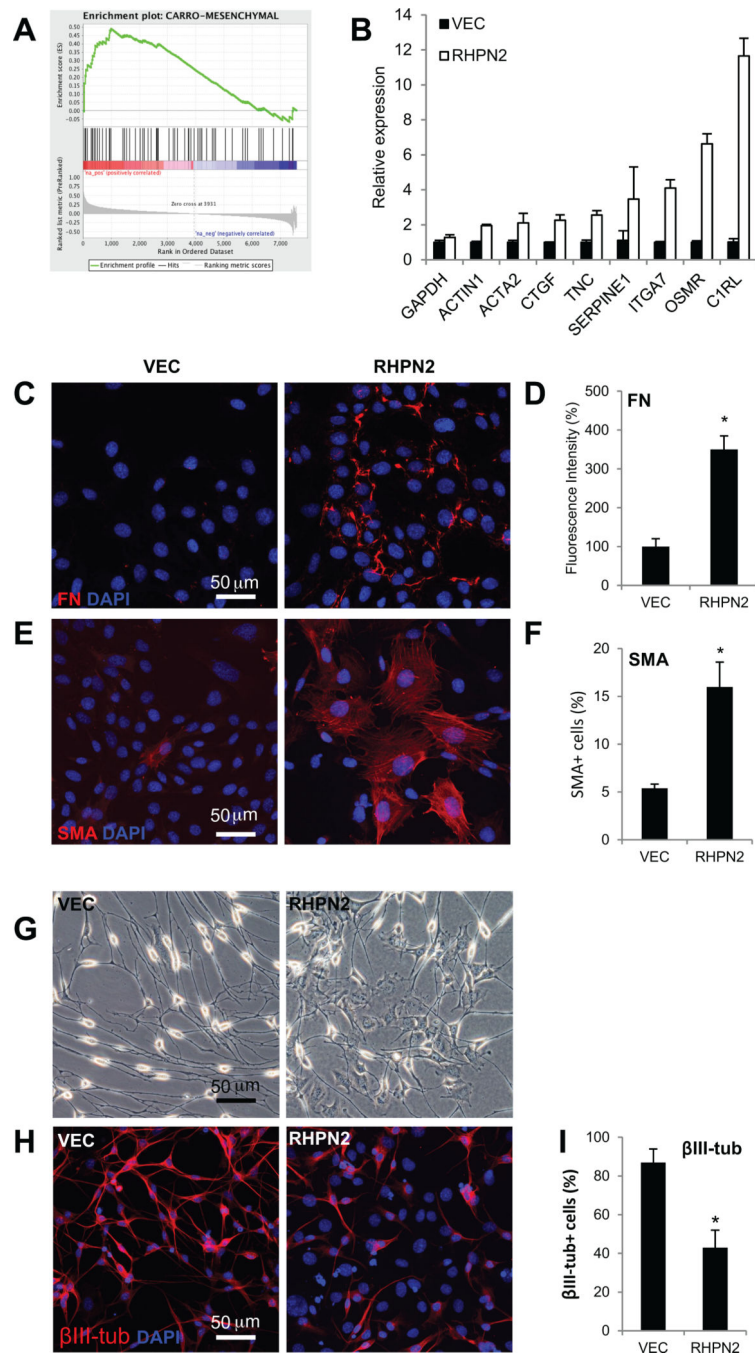
Figure 4. *RHPN2* induces MES transformation

(A) GSEA analysis of MES gene enrichment on the gene expression profile of C17.2 upon *RHPN2* overexpression. The bar-code plot indicates the position of the MES genes; red and blue indicate a positive and a negative correlation, respectively (p- value = 0.0003).

(B) qRT–PCR of MES targets in C17.2 cells. Mean values ± SD of three experiments are reported.

(C) Immunofluorescence analysis of fibronectin (FN, red) on C17.2 expressing the control pLOC vector (VEC) and *RHPN2*. Nuclei are stained with DAPI (blue). Scale bar: 50 μm.

(D) ImageJ quantification analysis of C17.2 produced FN. Mean values ± SD of 20 fields per each condition, are reported. *p-value $< 1\times10^{-4}$.

(E) Immunofluorescence analysis of smooth muscle actin (SMA, red) on C17.2. Nuclei are stained with DAPI (blue). Scale bar: 50 μm.

(F) Quantification analysis of SMA-positive C17.2 cells. Mean values ± SD of 10 fields per each condition, are reported. *p-value $< 1\times10^{-4}$.

(G) Morphology of C17.2 cultured in absence of mitogens for 5 days. Scale bar: 50 μm.

(H) Immunofluorescence for βIII-tubulin (red) of C17.2 cells after 5 days of differentiation. Scale bar: 50 μm.

(I) Quantification of C17.2 βIII-positive cells. Mean values ± SD of 5 fields per each condition, are reported. *p-value $< 1\times10^{-4}$.
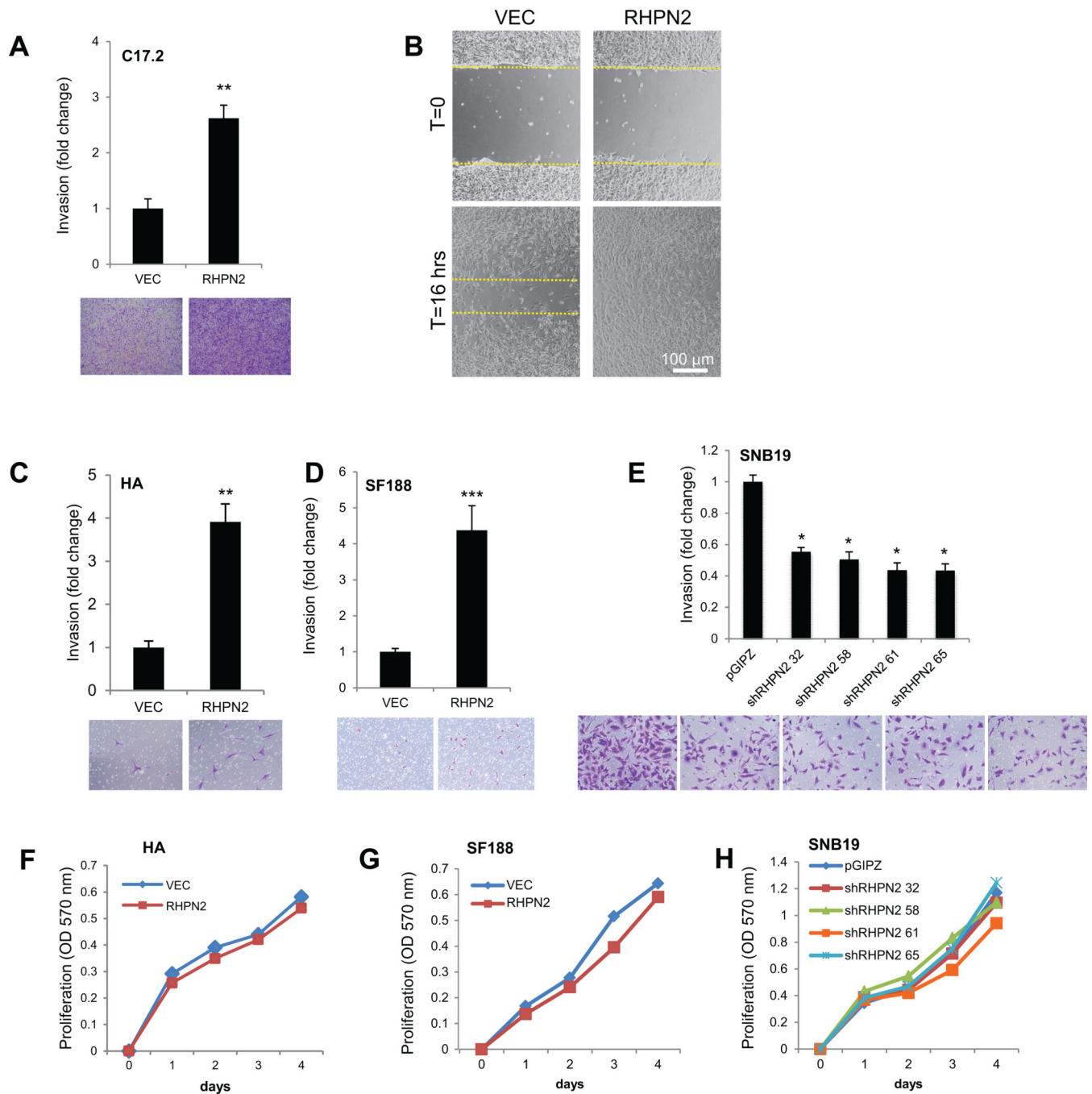
Figure 5. *RHPN2* promotes cell invasion

(A) Quantification of C17.2 invading cells. **p-value $< 1 \times 10^{-3}$.

(B) Microphotographs of C17.2 wound healing assay. Scale bar: 100 μm.

(C, D) Quantification of primary Human Astrocytes (HA) and SF188 invading cells at 24 hrs. **p-value $< 1 \times 10^{-3}$; ***p-value $< 1 \times 10^{-5}$.

(E) Quantification of SNB19 invading cells at 24 hrs, upon *RHPN2* silencing. *p-value < 0.005.

(F–H) Proliferation of HA, SF188 and SNB19 cells, upon overexpression or silencing of *RHPN2*.

All graphs in this figure show mean values and standard deviation of three repeats.
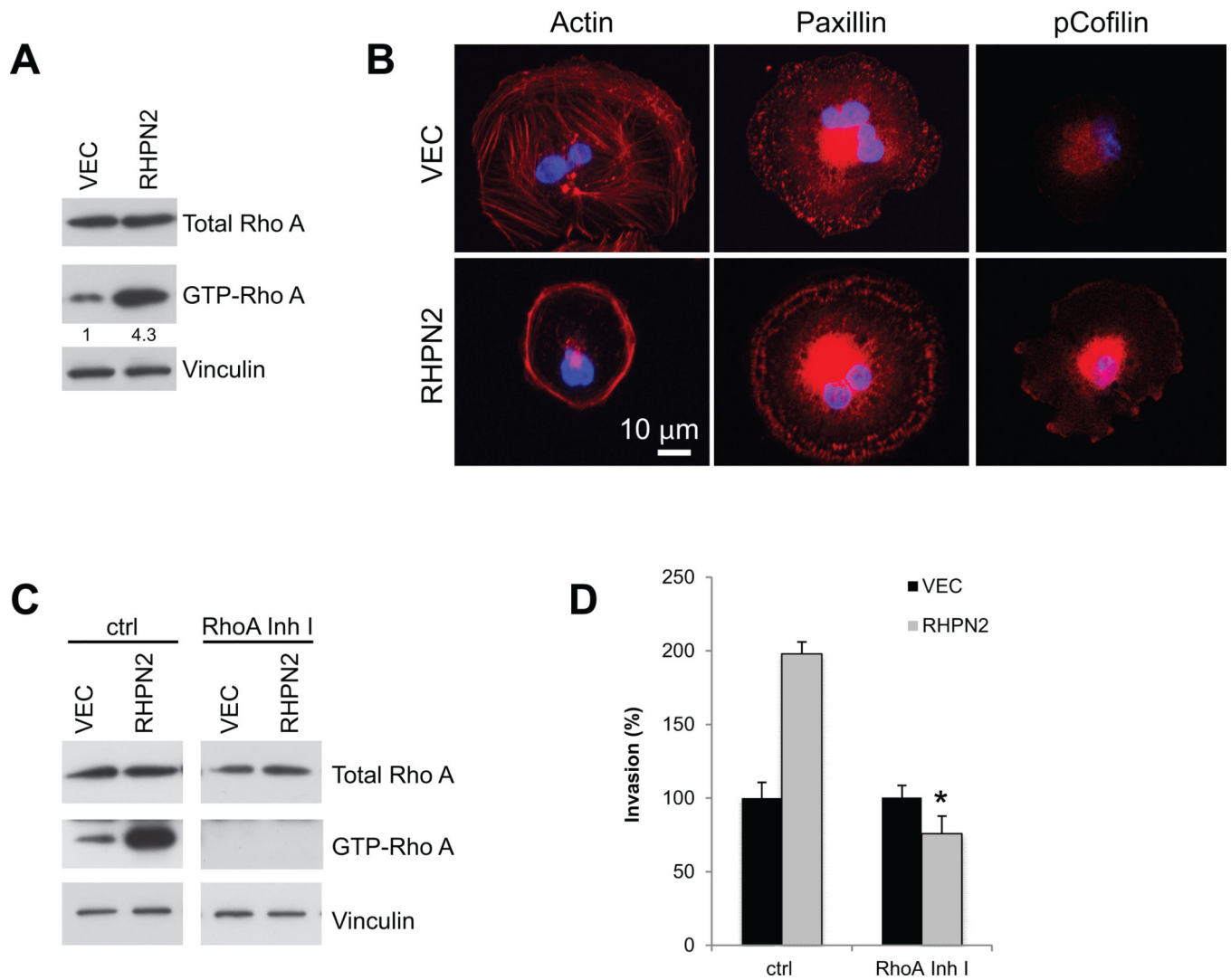
Figure 6. *RHPN2* induces a MES phenotype by triggering RhoA activation

(A) Rho activity assay of human astrocytes (HA) after 30 min of adhesion on Fibronectin (FN).

(B) Actin, Paxillin and pCofiln immunofluorescence staining (red) of HA after 30 min of adhesion on FN. Nuclei are stained in blue. Scale bar: 10 μm.

(C) Rho activity assay of HA. Cells were serum starved for 24 hrs and treated with 1 μg/ml of the RhoA inhibitor I for 6hrs. Untreated (ctrl) and treated (RhoA inh I) HA were then plated on FN for 30 min and harvested for RhoA analysis.

(D) Quantification of HA invading cells at 24 hrs. Cells were treated with 1 μg/ml of the RhoA inhibitor I. Mean values ± SD; n = 3; **p-value $< 3 \times 10^{-5}$.